Article

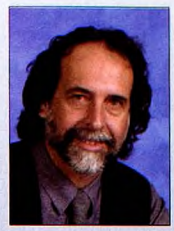

Airborne Electromagnetic Bathymetry Methods for Mapping Shallow Water Sea Depths

By Julian Vrbancich, Maritime Operations Division, Defence Science and Technology Organisation, Australia

Abstract

The Airborne ElectroMagnetic Bathymetry (AEMB) method is an emerging technique for estimating the sea depth and the seawater and sea bed electrical conductivities from the ElectroMagnetic (EM) response of the shallow water marine environment. The EM response is not affected by water turbidity and therefore the AEMB method can be used for bathymetric mapping in turbid waters. AEMB measurements can be taken from fixed-wing and helicopter systems for hydrographic reconnaissance and rapid environmental assessment. I review the basic principles of airborne electromagnetic systems that have been used for bathymetric mapping and present some examples of AEMB surveys in Australian waters.

Résumé

La méthode Bathymétrique ElectroMagnétique Aéroportée (AEMB) est une nouvelle technique d'estimation des conductivités électriques de la profondeur de l'eau, de l'eau de mer et du fond marin, à partir de la réponse ElectroMagnétique (EM) de l'environnement maritime peu profond. La réponse EM n'est pas affectée par la turbidité de l'eau et la méthode AEMB peut donc être utilisée pour la cartographie bathymétrique dans les eaux turbides. Les mesurages AEMB peuvent être effectués à partir de systèmes à voilure fixe et d'hélicoptères pour la reconnaissance hydrographique et l'évaluation environnementale rapide. Sont passés en revue les principes de base des systèmes électromagnétiques aéroportés qui ont été utilisés pour la cartographie bathymétrique, avec la présentation de quelques exemples de levés AEMB dans les eaux australiennes.

Resumen

El método de Batimetría ElectroMagnética Aerotransportada (AEMB) es una técnica emergente para estimar la profundidad del mar y las conductividades eléctricas del agua de mar y del fondo del mar, procedentes de una respuesta ElectroMagnética (EM) del entorno marino en aguas someras. La respuesta EM no se ve afectada por la turbidez del agua y, así pues, el método de AEMB puede utilizarse para representar la batimetría en aguas turbias. Las medidas de AEMB pueden tomarse a partir de sistemas de ala fija y de helicópteros para el reconocimiento hidrográfico y para una evaluación ambiental rápida. En este artículo reviso los principios básicos de los sistemas electromagnéticos que se han utilizado para la cartografía batimétrica y presento algunos ejemplos de levantamientos de AEMB en aguas australianas.

Introduction

The Australian Defence Science and Technology Organisation (DSTO) is investigating the Airborne ElectroMagnetic Bathymetry (AEMB) method to map seawater depth and seafloor conductivity in shallow water. This technique is expected to be particularly useful in turbid waters that attenuate light at optical wavelengths and prevent the effective use of LIDAR methods. Surveys have been conducted in coastal areas of hydrographic importance and include some or all of the following environmental features: turbidity, strong tidal flows in restricted and dangerous waters, shoals, channels and variable seafloor topography. This paper presents some results from several AEMB surveys in Australian waters.

Airborne ElectroMagnetic (AEM) surveying is used by the mineral exploration industry to detect ore bodies that may be buried beneath or within a conductive ground. Seawater also represents a conductive layer of 'ground' constrained to known upper and lower electrical conductivity limits, overlaying marine sediment layers and bedrock. Marine sediments have a lower electrical conductivity than seawater, and bedrock such as sandstone is resistive[1]. Thus AEM instrumentation and software developed for mineral exploration can be applied directly to survey the shallow water marine environment.

AEM uses a transmitting magnetic dipole source to generate a primary magnetic field that induces currents in the ground. These currents establish a secondary magnetic field (the EM response) that is detected by the receiver (Figure 1). A one-dimensional (1D) ground structure that consists of uniform infinitely planar layers of conductive or resistive material is usually assumed for AEMB mapping. EM software interprets the response in terms of layer thickness and resistivity of each layer. The basement is infinitely deep. The frequency response for a two-layer ground is discussed below. Numerical modelling usually assumes either a two-layer model (seawater over resistive basement) for estimating sea depth, or a three-layer model (seawater over unconsolidated marine sediment overlying resistive basement) for estimating sea depth and seafloor resistivity. AEM instrumentation can directly sample the resistivity of subsurface layers in shallow seawater.

Typical conductivity ranges for marine sandstone, sands, and clays are 0.02 – 0.3, 0.5 – 2.0, and 1.5 – 2.5 S/m respectively (Jackson et al., 1978; Bennet et al., 1983). Our AEMB investigations in Sydney Harbour have shown that the interpreted resistivities of layers directly below very shallow seawater (10m) can only discriminate between marine sand and exposed bedrock (Vrbancich et al., 2000b). This result was obtained using a relatively low power helicopter frequency-domain system. At deeper depths, it is only possible to detect the seawater-seafloor boundary. This is the maximum depth of investigation, which was shown to be about 30m for a helicopter AEM system (Vrbancich et al., 2000a). Fixed-wing AEM systems currently provide a maximum depth of investigation of about 70m in seawater (Vrbancich et al, 2004a, b).

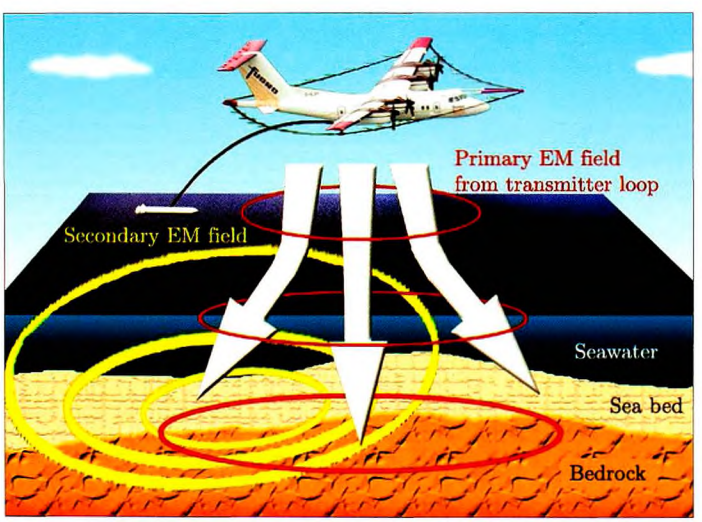

Figure 1: Schematic drawing of a time domain AEM system (GEOTEM) flying over shallow seawater. The primary magnetic field induces currents in the ground that generate a secondary magnetic field that is detected by the external receiver bird.

Becker, Morrison and co-workers pioneered the use of AEM for bathymet-

[1] The electrical conductivity (S/m) is the reciprocal of electrical resistivity (Ωm), and these terms are interchanged accordingly depending on whether one is discussing a good conductor or a poor conductor, e.g., seawater is conductive, bedrock is resistive

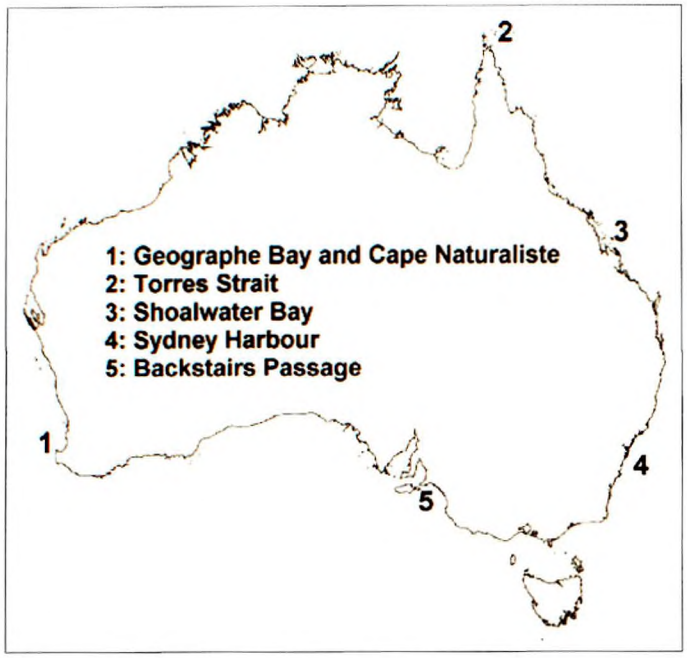

Figure 2: Locations of AEMB surveys in Australia.

ric mapping (Morrison and Becker 1982, Zollinger et al., 1987), and Won and Smits (1986) and Bergeron and co-workers (Bryan et al., 2003, Bergeron et al., 1989) have also investigated AEM bathymetry. Palacky and West (1991) have briefly reviewed AEMB, however to date, these methods have not been widely used for bathymetric mapping. AEM has also been used for mapping sea ice thickness (Kovacs and Holladay 1990; Liu and Becker, 1990). This application of AEM is possible because sea ice is two to three orders of magnitude less conductive than seawater and is therefore not detected by low frequency AEM instrumentation. The sea ice thickness is the difference between the height above seawater, which is estimated from AEM measurements, and the height above the ice surface determined from altimeter measurements. The sea ice thickness obtained from AEM measurements can be compared with accurate ground truth data in areas where the ice structure is known to be 1D, 2D or 3D. This comparison tests the accuracy of interpretation software used for bathymetric mapping and enables verification of AEM footprint sizes that determine the lateral resolution (Liu and Becker, 1990; Kovacs et al., 1995; Reid and Vrbancich, 2004).

AEM involves complex instrumentation systems and supporting software that is being developed by industry, government and academic research organisations. Australian AEMB survey locations were chosen in areas affected by turbidity (Shoalwater Bay, Torres Strait, Sydney Harbour), varying seafloor topography (Sydney Harbour, Backstairs Passage and Shoalwater bay), varying sea depth extending to deeper waters (Geographe Bay – Cape Naturaliste) and presence of shoals, reefs and very strong tides (Shoalwater Bay). The survey locations are shown in Figure 2.

Frequency Domain AEM System Response for a Two-layer 1D Earth

The expressions for the EM response in the frequency domain are given below, for coupled transmitter-receiver loop systems (Wait, 1982, Frischknect[2], 1967). Consider a Vertical Magnetic Dipole (VMD) transmitter, formed by a horizontal current loop system, at a height *h* above the origin over the surface of a two-layer ground as shown in Figure 3, and a receiver coil located at point P a distance *z* above the ground. Figure 3 also shows a Horizontal Magnetic Dipole (HMD) transmitter directed along the Y-axis. The magnetic field in free space is referred to as the primary field. The VMD primary field components are

$$(H_x)_p = \frac{3mx(z-h)}{4\pi r^5}$$

$$(H_y)_p = \frac{3my(z-h)}{4\pi r^5} \qquad (1)$$

$$(H_z)_p = \frac{3m(z-h)^2}{4\pi r^5} - \frac{m}{4\pi r^3}$$

[2] Frischknecht's article follows Wait's original papers that are contained in Wait (1982)

and the corresponding HMD components are

$$(H_x)_p = \frac{3mxy}{4\pi r^5}$$
$$(H_y)_p = \frac{3my^2}{4\pi r^5} - \frac{m}{4\pi r^3} \qquad (2)$$
$$(H_z)_p = \frac{3my(z-h)}{4\pi r^5}$$

where $r^2 = \rho^2 + (z-h)^2$, $\rho^2 = x^2 + y^2$, and the magnetic moment is $m = nIA$ where n is the number of turns, I is the loop current and A is the loop area. SI units are used throughout.

For the two-layer model (Figure 3), the secondary magnetic fields for the VMD case are (Wait, 1982, Frischknect, 1967)

$$(H_x)_s = -\frac{m}{4\pi\delta^3}\frac{x}{\rho}T_1$$
$$(H_y)_s = -\frac{m}{4\pi\delta^3}\frac{y}{\rho}T_1 \qquad (3)$$
$$(H_z)_s = -\frac{m}{4\pi\delta^3}T_0$$

and the corresponding secondary field components for the HMD case are

$$(H_x)_s = \frac{m}{4\pi\delta^3}\frac{xy}{\rho^2}\left(\frac{2}{B}T_2 - T_0\right)$$
$$(H_y)_s = \frac{m}{4\pi\delta^3}\frac{y^2}{\rho^2}\left[\left(1-\frac{x^2}{y^2}\right)\frac{T_2}{B} - T_0\right] \qquad (4)$$
$$(H_z)_s = \frac{m}{4\pi\delta^3}\frac{y}{\rho}T_1$$

where the electrical skin depth of the upper layer δ (m) is given by

$$\delta_1 = \left[\frac{2}{(\sigma_1 + i\varepsilon_1\omega)\mu_0\omega}\right]^{1/2} \approx \left(\frac{2}{\sigma_1\mu_0\omega}\right)^{1/2} \qquad (5)$$

and $k = \sigma_2/\sigma_1 = \delta_1^2/\delta_2^2$; $A = (z+h)/\delta$; $B = \rho/\delta$; $D = 2d/\delta$;

$$U = \sqrt{(g^2 + 2i)}\,;\; V = \sqrt{(g^2 + 2ik)}\,;$$
$$T_0 = \int_0^\infty Rg^2 e^{-gA} J_0(gB)dg$$
$$T_1 = \int_0^\infty Rg^2 e^{-gA} J_1(gB)dg \qquad (6)$$
$$T_2 = \int_0^\infty Rge^{-gA} J_1(gB)dg$$

and the complex reflection coefficient is

$$R = 1 - 2g\left[\frac{(U+V)+(U-V)e^{-UD}}{(U+g)(U+V)-(U-g)(U-V)e^{-UD}}\right] \quad (7)$$

In these expressions, i is the complex quantity $\sqrt{-1}$; μ_0 is the magnetic permeability of free space, ω is the angular frequency $(2\pi f)$; ε is the electrical permittivity of the upper layer, σ_1 and σ_2 are the electrical conductivities of the upper and basement layers respectively, J_0, J_1 are the zero'th and first-order Bessel functions of the first kind respectively and g is an integration variable. The approximation used in Equation (5), i.e. $\omega\mu_0\sigma \gg \omega^2\mu_0\varepsilon$ which is typically valid for frequencies f less than about 500kHz, implies that the Helmholtz diffusion equation can be used to describe the electromagnetic fields. This is referred to as the quasi-static approximation $\sigma/\omega\varepsilon \gg 1$ where conduction currents predominate. If $\omega^2\mu_0\varepsilon \gg \omega\mu_0\sigma$ (i.e., $\sigma/\omega\varepsilon \ll 1$) displacement currents predominate and the wave equation describes the electromagnetic fields. The extension to a multi-layered earth is given by Wait (1982).

The mutual coupling ratio (Z/Z_0) is defined as the ratio of the mutual coupling between a given source and receiver in the presence of the layered earth to the mutual coupling between the same source and receiver in free space. The ratio Z/Z_0 is equivalent to the ratio of the total field (primary and secondary fields) measured at the receiver to the primary field measured at the receiver, $Z/Z_0 = (H_s + H_p)/H_p$ (Frischknecht, 1967). AEM instrumentation measures the secondary field at survey altitudes, as well as the primary field at higher altitudes. The ratio of the secondary field to the primary field is provided by the survey contractor (after corrections have been made), expressed as parts per million (ppm), and is theoretically equivalent to $Z/Z_0 - 1$ assuming a one-dimensional ground.

For the Horizontal CoPlanar (HCP) transmitter-receiver geometry (VMD transmitter, coplanar receiver coil) with the receiver coil located along the Y-axis, ($x = 0$, $z = h$, $\rho = r = y$,, Figure 3), the receiver only detects the vertical field component, and from Equations (1, 3),

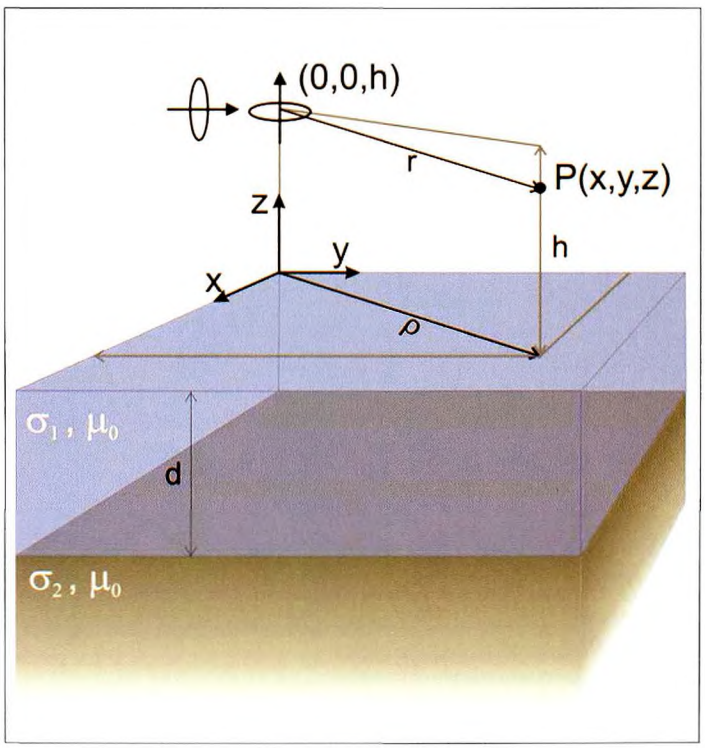

Figure 3: A Vertical Magnetic Dipole (VMD) represented by a circular current loop parallel to the X-Y plane is shown located above the origin, at a height 'h', over a one-dimensional (1D) two-layer non-magnetic ground. A Horizontal Magnetic Dipole (HMD) represented by a circular current loop parallel to the X-Z plane is also shown at the same location of the VMD. The receiver is located at point P, a distance z above the ground surface. The thickness of the upper layer is 'd'. The conductivity of the upper layer and basement is σ_1 and σ_2 respectively. μ_0 is the magnetic permeability of free space.

$$Z/Z_0 - 1 = (H_z)_s/(H_z)_p = B^3 T_0 \quad (8)$$

Similarly for the Vertical CoaXial (VCX) transmitter-receiver geometry (HMD transmitter, coaxial receiver coil) with the receiver coil lying in a plane parallel to the HMD transmitter coil, located along the Y-axis, the receiver only detects the horizontal Y-directed field component, and from Equations (2, 4),

$$Z/Z_0 - 1 = (H_y)_s/(H_y)_p = (B^2/2)(T_2 - BT_0) \quad (9)$$

As shown by Equations (8, 9), the integrals in Equation (6) contain all the information required to model the performance of inductively coupled loops. For a given system geometry and height above ground, the EM response for the two-layer ground at a given frequency is determined by the thickness of the upper layer (d) and the conductivities of the upper layer and infinitely deep basement, σ_1 and σ_2 respectively. For an equivalent M-layer ground, the EM response will be determined by the layer thicknesses $d_1, d_2 \cdots d_{M-1}$ and layer conductivities $\sigma_1, \sigma_2 \cdots \sigma_{M-1}, \sigma_M$. The fast numerical evaluation of these integrals, Equation (6), is very important for modelling and inversion of EM response data. The integration uses a fast Hankel transform procedure that involves numerical convolution using predetermined linear digital filter coefficients and is more than an order of magnitude faster than direct numerical integration and avoids evaluation of Bessel functions (Anderson, 1979; Johansen and Sorensen, 1979).

AEM Systems

AEM operates in either time domain (Transient ElectroMagnetic, TEM) or frequency domain (Frequency ElectroMagnetic, FEM). Fixed-wing systems usually operate in TEM mode and helicopter systems operate in FEM mode and more recently, in TEM mode. All three types of systems have been used by DSTO for AEMB surveys[3]. Fountain (1998) has reviewed the first fifty years of AEM development.

Frequency Domain AEM Systems

The FEM systems consist of several transmitter-receiver coil pairs in a fixed geometry where each transmitter operates continuously at a particular sinusoidal frequency and each corresponding receiver coil has been tuned to the transmitter frequency. The coil pairs are enclosed in a robust tube ('bird') suspended about 30m below the helicopter and about 30 to 40m above sea level. Survey speed and sampling rate is typically 60 knots and 10Hz respectively, or about 1 sample every 3m. The location at each sample is identified by a station or fiducial label. Lowering the operating frequency gives better penetration in a conductor (Equation (5), Table 1), but use of a single low frequency may be unsuitable because a range of frequencies are usually required to get depth resolution. Equivalently, in a time domain system, it is necessary to have a range of time-delayed channels to obtain depth resolution.

The transmitter-receiver coil pair separation is about 8 m or less, and the coils may be placed horizontally (Horizontal Co-Planar (HCP) configuration), or the coil pair may be rotated by 90°, so that the coils lie in the vertical plane (Vertical Co-Planar (VCP) configuration), or the coil axes lie on the same horizontal line (Vertical Co-aXial (VCX) configuration). With respect to the flight direction, the HCP, VCP and VCX coil configurations have the transmitter dipole moment aligned vertically, transversely and longitudinally respectively.

The first survey of Sydney Harbour used a DIGHEM^v system (Figure 4) which is an analogue instrument consisting of 5 coil pairs (3 HCP and 2 VCX, Table 1). The lowest frequency was tuned to 328Hz to maximise the depth of penetration through seawater. Since then, Shoalwater Bay and Sydney Harbour have been surveyed using an analogue DIGHEM_Res(istivity) instrument with 5 HCP coil pairs operating within

[3] The AEM systems GEOTEM, DIGHEM and TEMPEST, are trademarks of Fugro Airborne Surveys Pty Ltd. QUESTEM was operated by World Geoscience Corporation since 1990 and became obsolete in 2000 after the amalgamation of World Geoscience Corporation and Geoterrex-DIGHEM Pty Ltd into the newly formed company Fugro Airborne Surveys Pty Ltd

the range of 387 Hz to 103 kHz (Table 1).

Res_bird (Hz)	DIGHEM^{v} (Hz)	δ (m)	2δ (*)
	f_1=328 (HCP)	13.8	27.6
f_1=387 (HCP)		12.7	25.4
	f_2=889 (VCX)	8.4	16.8
f_2=1537 (HCP)		6.4	12.8
	f_3=5658 (VCX)	3.3	6.6
f_3=6259 (HCP)		3.2	6.4
	f_4=7337 (HCP)	2.9	5.8
f_4=25800 (HCP)		1.6	3.2
	f_5=55300 (HCP)	1.1	2.2
f_5=102700 (HCP)		0.8	1.6
nominal frequency	100	25.0	50.0
nominal frequency	45	37.3	74.6

(*) Depth of penetration equivalent to about 2 skin depths.

Table 1: Skin depths (δ) for DIGHEM frequencies and nominal frequencies.

Fixed-wing Time Domain AEM Systems

Fixed-wing TEM systems have the transmitter coil spanning the wingtips and front and rear extremities of the aircraft, as shown in Figure 5, with the receiver coil contained in a bird that is released from the rear of the aircraft. The transmitter and receiver operate at different heights above ground level. The aircraft survey altitude is about 120m and the bird has an assumed fixed horizontal offset within the range of 90 to 120m and a fixed vertical offset within the range of 40 to 60m, relative to the centre of the transmitter. At 120 knots survey speed, data processing leads to intervals of approximately 12m between samples. Variations in the assumed nominal fixed receiver offsets caused by swaying motion may lead to interpretation errors arising from unrecorded variations of bird attitude, offset and altitude. The magnetic dipole moment is the product of the loop area, the loop current and the number of turns of conductor forming the transmitter loop. A combination of large transmitter loop area and large pulsed transmitter current enables the TEM system to generally achieve much larger transmitter magnetic dipole moments than moments achievable in an FEM system.

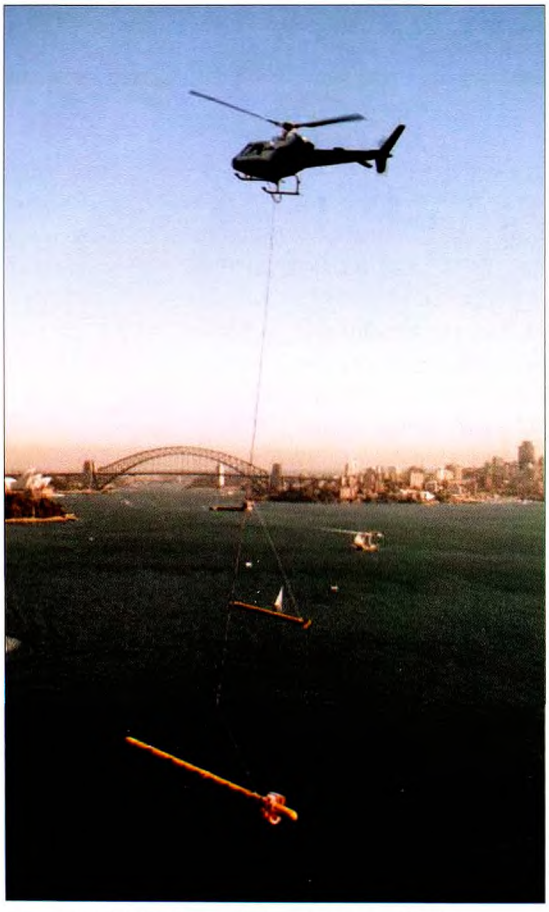

Figure 4: DIGHEM^{v} over Sydney Harbour, 1998.

The GEOTEM 25Hz system (Smith and Annan, 1997) has a transmitter waveform period of 40ms (25Hz) and only transmits a primary magnetic field during a 4ms current pulse having a half-sine waveform. After 16ms (the off-time duration with no transmitter current), this is repeated with the following transmitter pulse of opposite polarity. The receiver records the EM response in 15 off-time windows. A 12.5Hz base frequency system uses an 8ms current pulse and an off-time duration of 32ms. At early times, the first few windows record the higher frequency components of the EM response originating from the ground at relatively shallow depths. At the latest system times, the last windows record the lower frequency components of the EM response originating from the ground at relatively deeper depths. The longer the off-time period, the greater the time delay of recording channels, the

Figure 5: GEOTEM AEM system and an AEM bird deployment (inset).

lower the EM response frequency of the TEM system and therefore the greater the depth of penetration. Achieving lower operating frequency is difficult because of additional low frequency noise sources that contribute to the measured EM response. Geographe Bay and waters offshore from Cape Naturaliste (Western Australia) were surveyed using GEOTEM 25Hz and 12.5Hz systems to determine if the expected improvements offered by a lower base frequency could be achieved (Vrbancich et al, 2004b). Lane et al. (1998) discuss the QUESTEM 25Hz AEM system, which is similar to the GEOTEM 25Hz system, and associated data acquisition, signal processing and EM response waveforms. The TEMPEST system (Lane et al., 2000) also has similar features but is designed with a higher bandwidth and can therefore detect a higher frequency ground response than the GEOTEM and QUESTEM systems to provide better resolution of subsurface conductivity as is required for salinity mapping and possibly bathymetric mapping.

Helicopter Time Domain AEM Systems

An example of a helicopter TEM instrument is the HoisTEM system developed in Australia by Normandy Mining Ltd (now Newmont Mining Inc.). HoisTEM has been used in several DSTO surveys, including Sydney Harbour, see Figure 6. The HoisTEM structure contains a 24m diameter transmitter loop with an inner concentric loop as the receiver coil. This configuration only measures the vertical component of the secondary magnetic field, whereas fixed-wing TEM systems usually measure all three components. Of these three components, only the vertical and inline component EM responses are usually analysed.

Interpretation of Water Depths from AEMB Surveys

Two generic procedures, Layered-Earth Inversion (LEI) and Conductivity-Depth Imaging (CDI), are used to estimate water depths and seafloor resistivity from AEM data.

Inversion

A 1D frequency-domain inversion program developed by Fullagar for HCP coils (Fullagar and Oldenburg, 1984) was extended by Fullagar (program *AEMIE*) to support AEMB studies (Vrbancich et al., 2000b). The inversion is initiated with a starting model, consisting of layers with a given thickness and conductivity on a basement of fixed conductivity. During inversion, the layers can be split and layer splitting can occur more than once, until a specified maximum number of layers are attained. The quality of the data and the assumption of a layered subsurface will govern the achievable degree of fit between observed and modelled data. Other programs used to forward model time-domain and frequency-domain AEM data for 1D layered earth and 2D, 3D targets, and to invert data for a 1D layered earth, have been developed by Raiche and coworkers (e.g., Raiche, 1999; Raiche et al., 1996). These programs form part of a suite of programs developed as part of the AMIRA International Project P223 (Advanced EM Modelling Software), of which DSTO is a contributing sponsor. These programs are under continual development and have been used to interpret frequency and time domain AEMB data. Fugro Airborne Surveys Pty Ltd also inverts DIGHEM, QUESTEM and GEOTEM AEM data using proprietary in-house software.

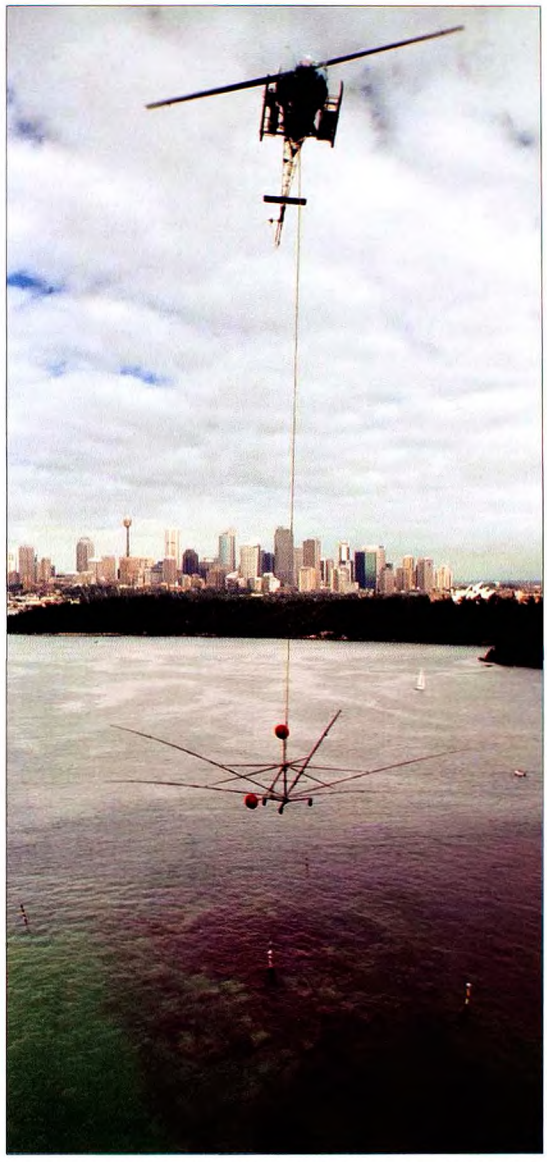

Figure 6: HoisTEM AEM system over Sow and Pigs reef, Sydney Harbour, 2002.

Conductivity-Depth Imaging (CDI)

The Conductivity-Depth Imaging (CDI) process was developed to enable faster processing of AEM data, but is less accurate than least-squares inversion because it is based on image theory and moving 'smoke rings' of electric current diffusing into the ground. For TEM data, the initial stage involves deconvolution to a single step response where EM response data from an arbitrary transmitter current waveform is transformed to the tau (time constant) domain. The step response has the waveform dependence of the AEM system removed and now consists of a series of decaying exponential functions with different time constants and different initial amplitudes. The range of time constants covers the range of delay times being sampled by the AEM system. This allows generic algorithms to be used for data processing rather than waveform specific algorithms. An equivalent procedure also exists for frequency domain data.

The basis of (CDI) processing then is to determine an equivalence between a set of conductivities and a set of delay times such that the magnetic field of an image dipole at a given depth equals the computed step response at a given delay time. Here, the image dipole depth is the sum of the transmitter height and the penetration depth at the given time, and the penetration depth is assigned to a given conductivity. Conductivities are fitted parameters that are varied during the CDI processing and there is an implied relation between time delay and penetration depth (Wolfgram and Karlick (1995). This CDI method is

based on the Maxwell receding image concept (Macnae and Lamontagne, 1987; Macnae et al., 1991). Macnae and co-workers have incorporated the Maxwell receding image technique into a CDI processing program called *EMFlow*, developed as part of the AMIRA International Project P407 (Geologically Constrained Automatic and Interactive Interpretation of EM Data), of which DSTO is a contributing sponsor.

Another CDI method developed by Fullagar involves the determination of apparent conductivity at each TEM delay time, followed by the estimation of the apparent depth as the depth of maximum current (and hence maximum electric field) in a half-space with conductivity equal to the apparent conductivity at the delay time in question (Fullagar and Reid, 1992). This procedure has been incorporated into the program *Emax*. Both *EMflow* and *Emax* have been used to interpret AEMB data (Vrbancich et al, 2000b.; Vrbancich and Fullagar, 2004). Rapid automatic methods for detecting abrupt changes in the variation of conductivity with depth are being investigated to define conductivity boundaries in CDI processed data including the seawater-seafloor boundary for bathymetric mapping (Macnae et al., 2004).

AEMB Surveys – Sydney Harbour

The seafloor terrain of the surveyed region in Sydney Harbour (Port Jackson) is varied and includes a reef straddled by two shipping channels, plane areas, relatively deep troughs, and an area of shallow potholes. Sydney Harbour was used as a test area to showcase side-scan sonar, multi-beam echo-sounding, seabed classification and laser airborne depth sounding technologies. The data from these surveys provided a common database for the International High Resolution Surveys in Shallow Water conferences held in Sydney in 1997 and 2003. This information, combined with marine seismic data (Emerson and Phipps, 1969; Harris et al., 2001) that estimates the depth to bedrock and sediment thickness, provides a substantial ground-truth database for supporting AEMB studies.

DIGHEM^{V} Survey

The DIGHEM^{V} survey of Sydney Harbour took place in 1998 in calm weather (Figure 4) and consisted of twenty one parallel profiles flown with a nominal line spacing of 50m (Vrbancich et al., 2000a). Each profile is approximately 5.5km long. The survey region is shown in Figure 7. The results of using a two-layer inversion (Fugro Airborne Surveys proprietary software) to interpret water depth for line L20140, which passes directly over the Sow and Pigs reef, are shown in Figure 8. The two-layer inversion assumes a two-layer ground (Figure 3). The four model parameters are the resistivities of the upper seawater layer and basement, upper layer thickness (water depth) and bird altitude. Of the five DIGHEM frequencies, only data recorded at HCP 328Hz, 7337Hz and VCX 889 Hz were used for the inversion. The inverted basement resistivity over all flight lines was 0.6 Ω m, which is representative of marine sands. Inversion stability was also improved using a fixed seawater conductivity of 0.265 Ω m (3.8 S/m, about 20% less than the measured value) rather than allowing seawater conductivity to float during the inversion. The FAS-inversion sea depths were shown to be accurate, on average, to within about 2.6% in areas shallower than 10m (Vrbancich 2000a).

Figure 8 shows the inverted depths, accurate depths from acoustic soundings, estimated depths to bedrock and the residual (i.e., the difference between acoustic and AEMB depths). The difference in the spatial resolution between acoustic and AEMB methods increases the residual in sloping terrains, e.g., at 1,250 and 1,840m. The inverted depths track the known depths down to about 30m, except in two sections: (i) the northeast section is too deep (arising possibly from weak discrimination between seawater and water-saturated marine sand) and finishes abruptly too shallow (from incorrect data leveling), and (ii) the southwest section (0 to 400m) shows signs of mathematical instability in the inversion resulting in large unrealistic oscillations.

The footprint of the HEM system, the homogeneity of the 'geology' and sampling rate, will determine the spatial resolution of the AEMB method. Liu and Becker (1990) have calculated that the footprint of a VCX

Figure 7: DIGHEM^{V} survey lines, Sydney Harbour. Lines 20010, L20020 lie on the western side, skirting Middle Head (MH), Georeges Head (GH), Chowder Head (CH) and Bradleys Head (BH). The northeastern section of the survey area cuts across the harbour entrance to the east and stops at North Head (NH). Depth to bedrock contours (Emerson and Phipps, 1969) are shown at 15m intervals. The insert shows an enlarged area (scaled by a factor of 2) surrounding the Sow and Pigs reef. Line L20140 flies over this reef. The Western Channel is located approximately between the western boundary (Georges Head to Middle Head) and the Sow and Pigs reef area.

and HCP system is 1.35 and 3.73 times the transmitter height respectively (40 m and 112m respectively for a bird altitude of 30m). For a GEOTEM system (transmitter height = 120m, receiver height = 70m), the footprint is estimated to be 2.97 and 4.51 times the transmitter height for inline and vertical component data respectively (Reid and Vrbancich, 2004). The non-homogeneity of the geology can reduce the footprint/altitude ratio because the footprint definition averages areas of higher current density with areas of weaker current density. This implies that AEM anomalies may be affected by a structure at much smaller scales than the footprint.

The inverted depths from all AEMB profiles were gridded to map the seafloor topography. Depth soundings from single-beam surveys have been similarly gridded and are shown in Figure 9 together with gridded AEMB data, all with the same vertical exaggeration and colour scale. Overall, there is very good agreement between the two images. The AEMB image is compared with the equivalent image in Figure 10 that was obtained from laser depth soundings. Figure 10 shows a low-resolution 3D image from gridded laser

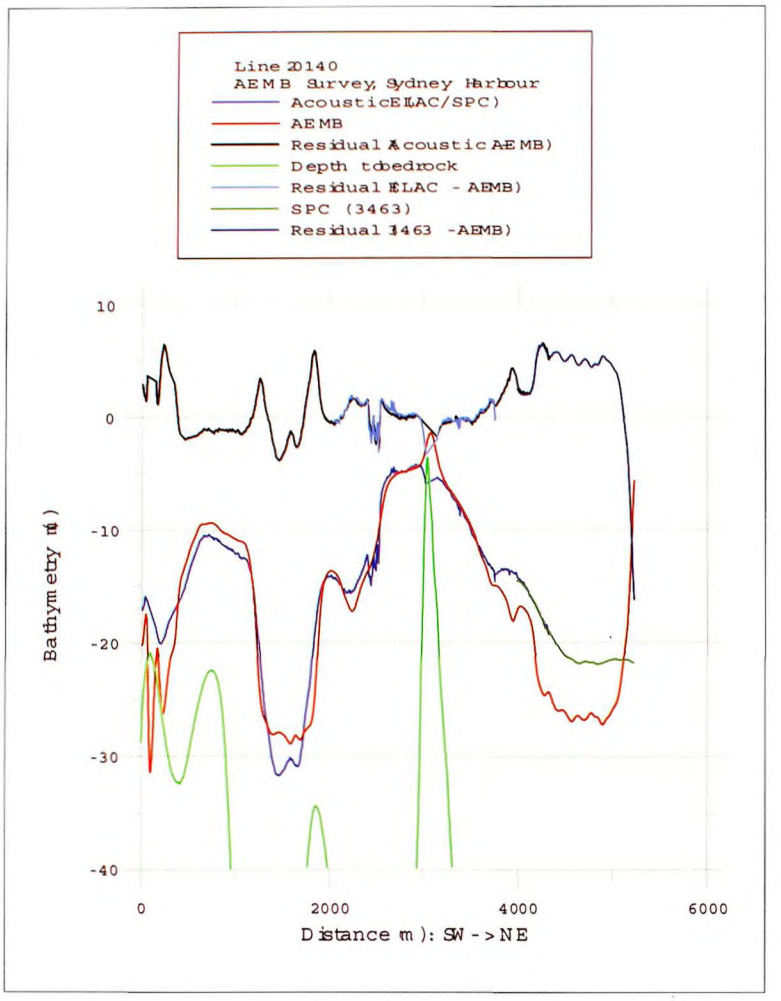

Figure 8: Bathymetry profiles, depth to bedrock profiles and residuals, L20140. Single-beam and multi-beam: 'Acoustic (ELAC/SPC)'; single-beam opposite harbour entrance: 'SPC (3463)'.

airborne depth sounding (LADS) bathymetry data provided by the Australian Hydrographic Service (AHS), as part of the common dataset for the 2003 High Resolution Surveys in Shallow Water conference. The LADS survey covers the same area as the AEMB survey and was flown in good conditions, see insert in Figure 10. Data was collected inside the harbour starting from North Head (Figure 7) and extending south across the Sow and Pigs reef and continuing to the vicinity of Shark Island (Figure 7) and finishing at about the southeastern corner of Figure 6. As shown in Figure 10, south of the reef and Western Channel, and in the Deviation Cut area, LADS data was unsuitable for bathymetric mapping because of water turbidity and poor reflections from the seafloor in these areas. In this survey, LADS depths appear limited to about 18m in areas where the marine sand provides good reflections.

Conductivity-Depth Sections: Bathymetry

Three representative lines of DIGHEMV data (L20010, L20020 and L2014, Figure 7) processed using layered earth inversion (AEMI) and CDI (EM Flow) methods to generate conductivity-depth sections are shown in Figures 11, 12. L20010 and L20020 profiles pass along the western side of the survey area adjacent to several headlands (Figure 7) where marine bedrock is exposed or lies just below the seafloor. L20140 passes over the Sow and Pigs reef near the centre of the survey area (Figure 7). The bathymetry profiles and bedrock depth profiles included in the conductivity-depth section images show sediment thickness variations along the flight paths. Details of the inversion parameters and CDI methods for this case study can be found in Vrbancich et al. (2000b).

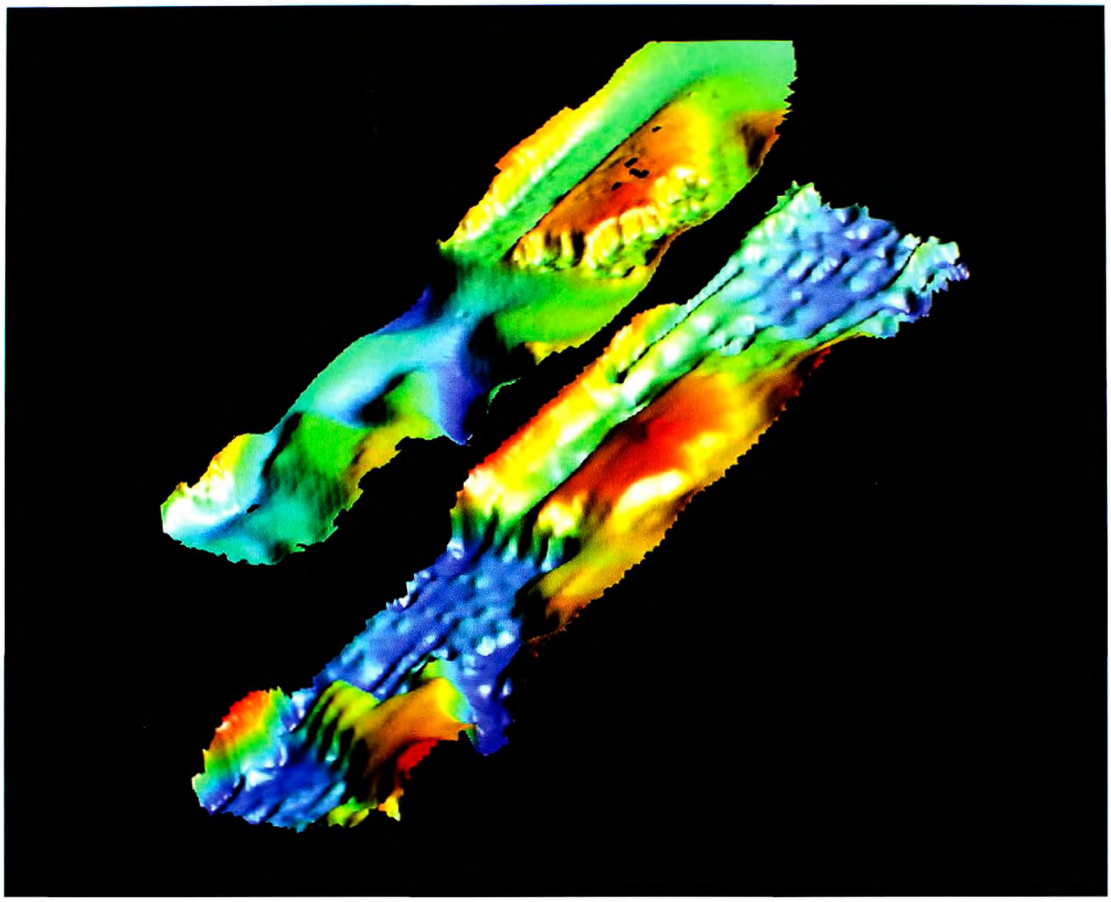

Figure 9: Digital seafloor terrain map of a portion of Sydney Harbour, showing the varied seafloor topography. Upper image represents combined single-beam and multi-beam sonar data. Lower image represents AEMB data. Both images are vertically aligned, with a vertical exaggeration of 14, and are colour draped to show the bathymetry: red (-4m), yellow (-12m), aqua to light blue (-16 to -20m) and dark blue (-32m). The major peak in the lower image is the tip of the Sow and Pigs reef which is too shallow to be surveyed using hull mounted sonar.

If conductivities greater than about 2.5 S/m are attributed to seawater, the inverted conductivity versus depth sections (AEMIE, Figure 11) for all 3 lines are in good agreement with the known water depth over most of the survey area, even in the deepest (30m) regions. The EM Flow results (Figure 12) are similar to the AEMI results. For L20010 (Figure 12a) between 6253000 mN and 6253400 mN, the agreement with estimated depth of about 18 to 20m is very good, as is the agreement with echo soundings between 6255600 mN and 6256300 mN at about 15 to 20m depth. The 32m depth at 6254000 mN and 25m depth between 62534000 mN and 6253900 mN is underestimated by EM Flow. For L20020 and 20140 (Figure 12a, b), there is generally good agreement with measured depth soundings, especially to depths of about 20m.

Conductivity-Depth Sections: Sediment and Bedrock

The conductivity-depth sections identify shallow regions of bedrock (associated with a conductivity less than 0.3 S/m) and layers of sediment (associated with a conductivity range between about 0.3 S/m and 2 S/m). The conductivity-depth sections for L20010 (Figures 11a, 12a) correctly identify the locations and approximate depths of the marine sandstone basement ridges extending out from Bradleys Head and Georges Head (Figure 7). AEMI sections predict shallow bedrock at about 15m depth opposite Middle Head. Recent marine seismic recordings (Harris et al., 2001) confirmed this prediction and have cor-

rected the depth to bedrock profile opposite Bradleys Head for L20020 (Figure 11 b) to show the location of the bedrock ridge to be in agreement with conductivity-depth sections. The marine bedrock ridges associated with Bradleys Head, Georges Head and Middle Head are detectable because they are located beneath very shallow water whereas the bedrock ridge extending from Chowder Head is not detected. Between 6254200 mN and 6254800 mN (L20020), the thickness of the interpreted sediment wedge (orange tones, Figures 11a, 12a) increases from about 10m, to 40m, in approximate agreement with the interpreted bathymetry and seismic boundaries.

The main feature in L20140 is the bedrock peak associated with the Sow and Pigs reef (Figure 7) at 6254400 mN (Figures 11c, 12c). The flanks of this feature are correctly defined by the sediment-basement contact (orange-blue transition) to a depth of about 40m. Both conductivity sections (Figures 11c, 12c) underestimate the expected bedrock conductivity that forms the reef.

HOISTEM Survey

The HoisTEM survey area overlies the DIGHEM survey area shown in Figure 7. CDI processing using program Emax (Fullagar and Reid, 1992) incorporating variable transmitter current is used to perform the conductivity-depth transform. Resulting CDI sections show that water depth can be estimated to a certain degree of accuracy however layered earth inversion for a three-layer earth (two layers over basement) gave improved agreement with known sea depths (Vrbancich and Fullagar, 2004). Figure 13 shows the conductivity depth section for line 1025, which is close to the third northeastern line of the survey area in Figure 7. Figure 13 shows that the relatively small tide correction of 1.4m is important for water depths less than 22m at the time of survey. In this case, inverted sea depths from AEM data achieve sub-metre accuracy. Between 22 to 25m water depths, inverted depths underestimate known depths by about 2m, and at 30m water depths, the residual increases to about 6m. This analysis is based on incorrectly calibrated HoisTEM data as supplied by the survey contractor. Layered earth inversion of some recalibrated HoisTEM data suggests that accurate inverted water depths can be obtained to depths of about 55m. These preliminary results suggest that comparable depths of investigation can be achieved using fixed-wing and helicopter AEM systems.

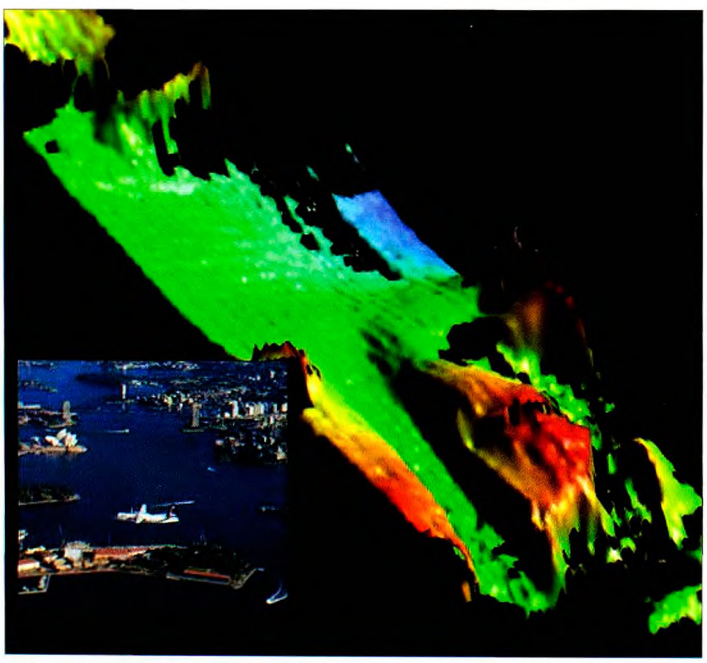

Figure 10: Photo (inset) of Royal Australian Navy Laser Airborne Depth Sounding (LADS) survey flown over Sydney Harbour, 17 May 2002, in good conditions. The low-resolution LADS bathymetry image extends from the harbour entrance to Sow and Pigs reef and Western Channel (Figure 7).

AEMB Survey - Shoalwater Bay

The Shoalwater Bay (SWB) area includes numerous shoals, reefs, and large tidal flows that stir up the muddy seafloor causing high levels of water turbidity. The DIGHEM_Resistivity bird surveyed three adjoining areas (Figure 14) in weather conditions that were generally windy (often in excess of 20 knots) and rainy with squalls leading to reduced visibility (Figure 14, inset). The survey showed that deployment of AEMB equipment and subsequent surveying can be undertaken in poor weather conditions and in areas of high turbidity. Single-beam depth sounding data

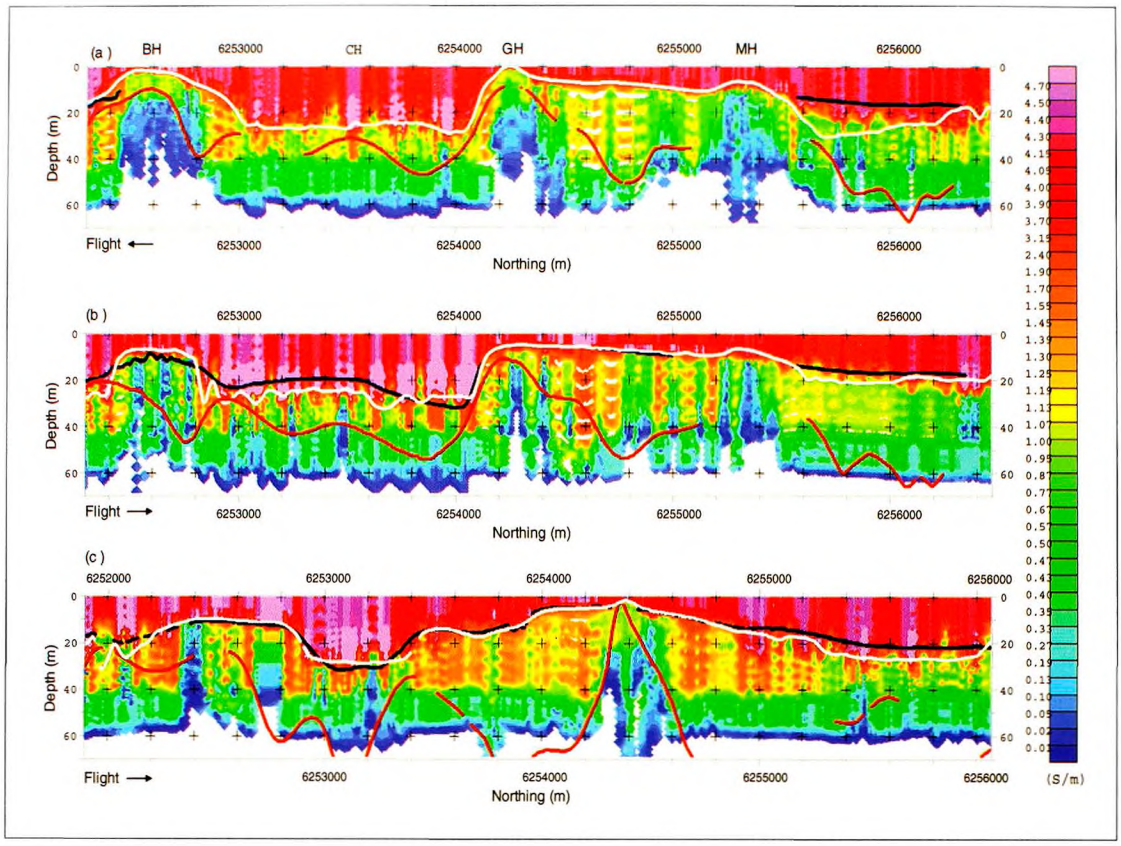

Figure 11: AEMI conductivity sections (S/m) with profiles of depth to bedrock from seismic surveys (Emerson and Phipps, 1969; red), echo-sounding water depths (black) and FAS-inversion water depths (white): L20010 (a), L20020 (b) and L20140 (c). Proximity of sandstone promontories in L20010: BH, Bradleys Head; CH, Chowder Head; GH, Georges Head and MH, Middle Head.

was provided by the AHS. Layered-earth inversion of AEM data gave good agreement (within 10%) with known water depths shallower than 18m in all three areas. This Section focuses on apparent resistivity, rather than CDI processing and layered earth inversion of AEM data. Apparent resistivity maps can be generated very quickly and have the potential to provide useful information that highlights resistive features in shallow seawater thereby identifying submerged rocks and very shallow seawater.

Apparent Resistivity

The apparent resistivity is the resistivity of a uniform ground that gives the same EM response as the response of a complex ground structure. The apparent resistivity is computed during the survey as a quick check on data quality. If the AEM frequency is high so that there is little penetration through seawater (i.e., a small skin depth, Equation (5), Table 1), then AEM only detects the seawater layer and is 'blind' to the resistive sea bottom. The apparent resistivity would therefore be expected to be that of seawater. If the AEM frequency is lowered so that the transmitted magnetic field passes through the shallow seawater layer with very little attenuation (i.e., a larger skin depth, Table 1), then AEM only detects the resistive sea bottom. In shallow seawater, depending on depth, apparent resistivity maps at the lowest DIGHEM frequency would be expected to show spatial variations that outline changes in water depth and resistive features of the seafloor topography.

In the following apparent resistivity maps, tidal variations involving 6 to 8m tides need to be taken into account because adjacent survey lines were not necessarily flown in consecutive order. The single-beam

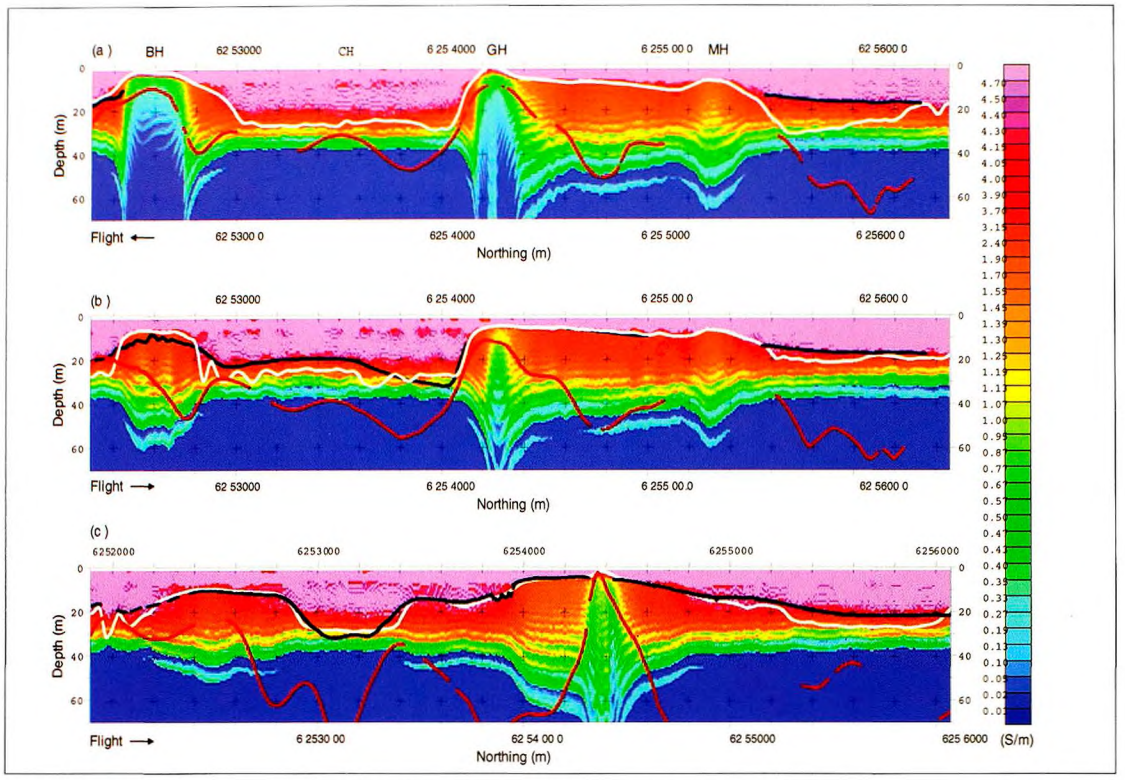

Figure 12: EM Flow conductivity sections (S/m) with profiles of depth to bedrock from seismic surveys (Emerson and Phipps, 1969; red), echo-sounding water depths (black) and FAS-inversion water depths (white): L20010 (a), L20020 (b) and L20140 (c). Proximity of sandstone promontories in L20010: BH, Bradleys Head; CH, Chowder Head; GH, Georges Head and MH, Middle Head.

echo soundings covering Area 1 were gridded and mapped as shown in Figure 15. Figure 16 shows the distribution of apparent resistivity at 387Hz and at 1,537Hz (12.7m and 6.4m nominal skin depths, respectively), which are the two lowest frequencies used in the AEMB survey (Table 1). The 'striped' discontinuous features through the centre of the region at 387Hz arise from 6 to 8m tides that cause variations in apparent resistivity. The difference between the two apparent resistivity maps shows that for shallow water, the lowest nominal DIGHEM frequency can be used to highlight variations in resistivity caused by corresponding variations in water depth. At 1,537Hz, the skin depth is too small to allow suitable detection of the sea bottom. The 'blue' areas in both maps in Figure 16 correspond to conductivities greater than or equal to 4 S/m, i.e., seawater.

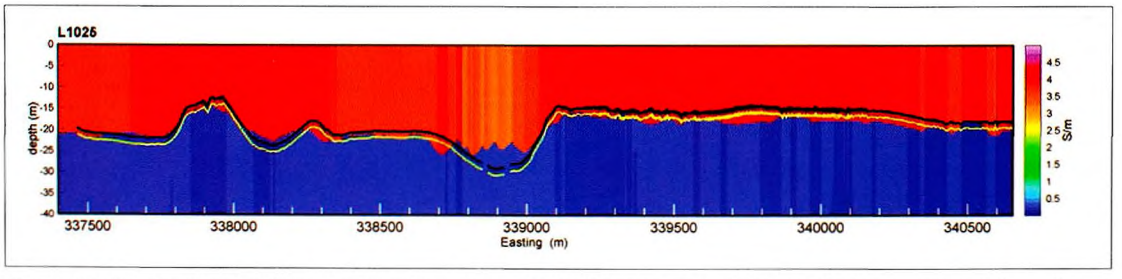

Figure 13: Conductivity-depth section from inversion of HoisTEM data for line L1025. The inversion model consists of two layers overlying a resistive basement. Accurate bathymetry profiles show tide-corrected depths (black) and depths at time of survey (yellow) accounting for a 1.4m tide.

There is a close resemblance between the 387Hz apparent resistivity for Area 1 (Figure 16) and the bathymetry map (Figure 15). This similarity would be improved if the AEM survey could have been flown with consecutive flight lines to minimise the effect of variations in sea depth on apparent resistivity at low frequency, caused by large tides. 3D images of the apparent resistivity are shown in Figures 16 (insets). The highly resistive areas correspond to headlands, and rocky areas near the shores that are submerged. The central areas highlight submerged rocks.

The apparent resistivity at 387 Hz for Area 2 (Figure 17) shows a discontinuity along the centre caused by the discontinuity in the tide. Comparison of Figures 14 and 17 shows that all of the charted submerged rock features in this area are identified at these shallow water depths. The largest area of high resistivity located along the middle on the discontinuity (Figure 17) decreases in area further north because the tide has now changed from 1m to 6m and the large rock feature (maximum drying height of 5.8m to the northern boundary of the survey region, Figure 14) is now covered by several metres of seawater. Regions of very shallow seawater are also clearly identified by the apparent resistivity maps.

Area 3 (Figure 14) lies between a beach on Townshend Island flanked by higher ground (north), and low lying Triangular Islands (south). The survey lines fly completely over the southwest island of Triangular Islands. The 3D apparent resistivity map at 387Hz (Figure 18) shows (i) the variations in resistivity to the beach approaches, (ii) the small variations in seawater depth across this section of Strong Tide Passage that are correlated with chart bathymetry contours (Figure 14) and (iii) the differences between the resistive headlands flanking the beach on Townshend Island and the less resistive regions around the low-lying Triangular Islands.

Apparent resistivity must be used with caution because the resistivity of an infinitely deep uniform 'ground' does not correspond to reality, yet as shown in these examples, it can discriminate between sea

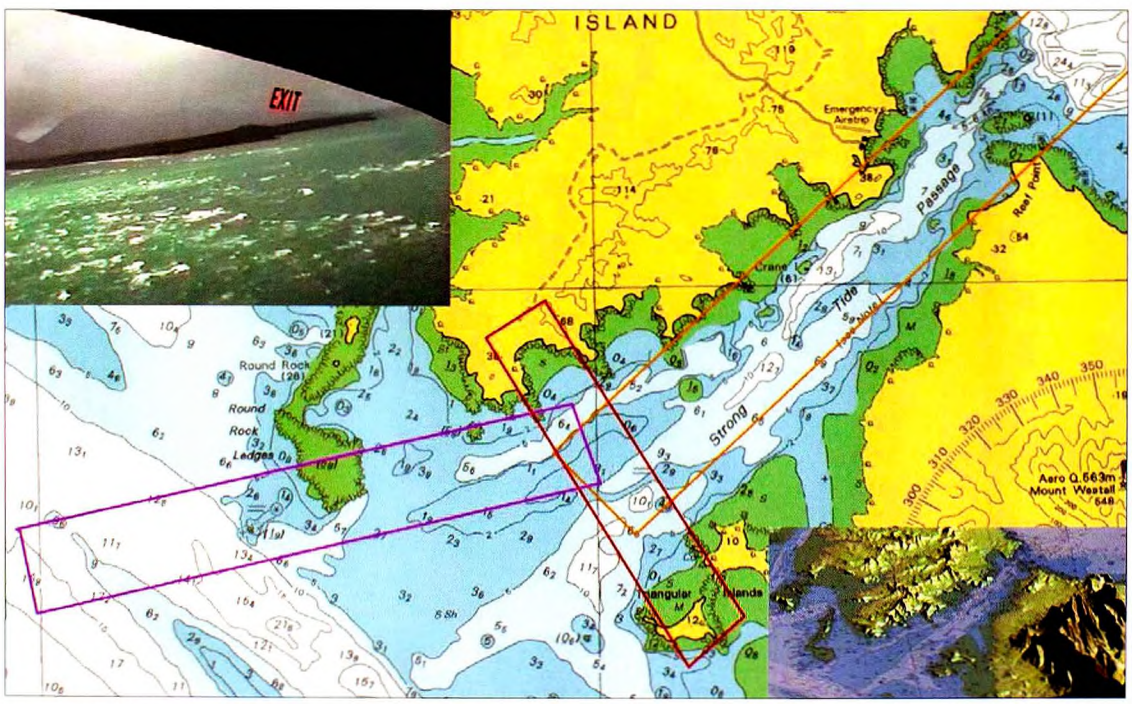

Figure 14: Shoalwater Bay survey areas. Area 1 (orange), Strong Tide Passage, 11.0km long; Area 2 (magenta), within Shoalwater Bay, 8.8km long; Area 3 (red), 5.5km long, linking Townshend Island (north) and Triangular Islands (south). Upper inset: photo of southeast headland of Townshend Island, photographed exiting Strong Tide Passage during survey of Area 1. Lower inset: Section of chart AUS260 draped over digital terrain elevation data to show relief of surveyed areas extending over land.

depths separated by a few metres in very shallow water and can also reveal submerged resistive features in shallow water. Dispersed bubbles in seawater would not affect the EM response and associated apparent resistivity because the bulk conductivity of the seawater would remain unchanged. AEMB measurements would therefore be expected to prove useful for bathymetric mapping in the surf zone.

AEMB Surveys – Geographe Bay and Cape Naturaliste

Geographe Bay and adjoining Cape Naturaliste (Figure 2) have been surveyed using the fixed-wing GEOTEM and QUESTEM TEM systems to determine the accuracy of bathymetric mapping and the maximum depth of investigation. Two vector components of the dB/dt EM response were analysed: the inline component (dBx/dt), parallel to direction of flight, and the vertical component (dBz/dt). Figures 19 and 20a show the depths obtained from the 25Hz QUESTEM and 25Hz GEOTEM surveys for the same flight path that starts in Geographe Bay in 30m of water, skirts Cape Naturaliste, and continues into deeper waters offshore from the cape (Vrbancich et al., 2004b). Figure 19 compares the interpreted depths from CDI processing using EMFlow, and inverted depths using layered-earth inversions (FAS-proprietry and from project P223) with known ground truth. The base depths of the vertical component CDI section accurate-

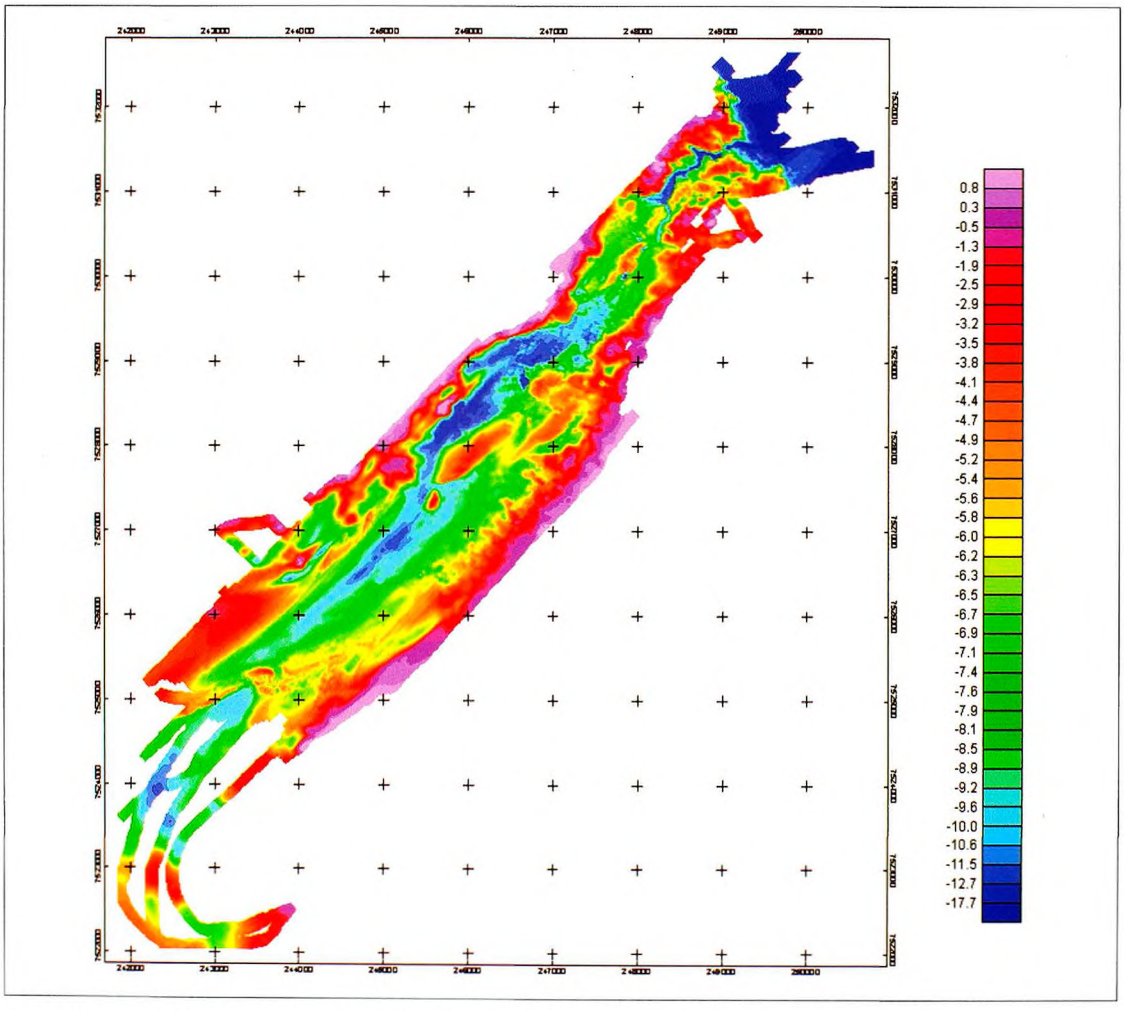

Figure 15: Gridded bathymetry map from single-beam echo soundings. Grid spacing is 1,000m, colour scale bar shows depth in metres.

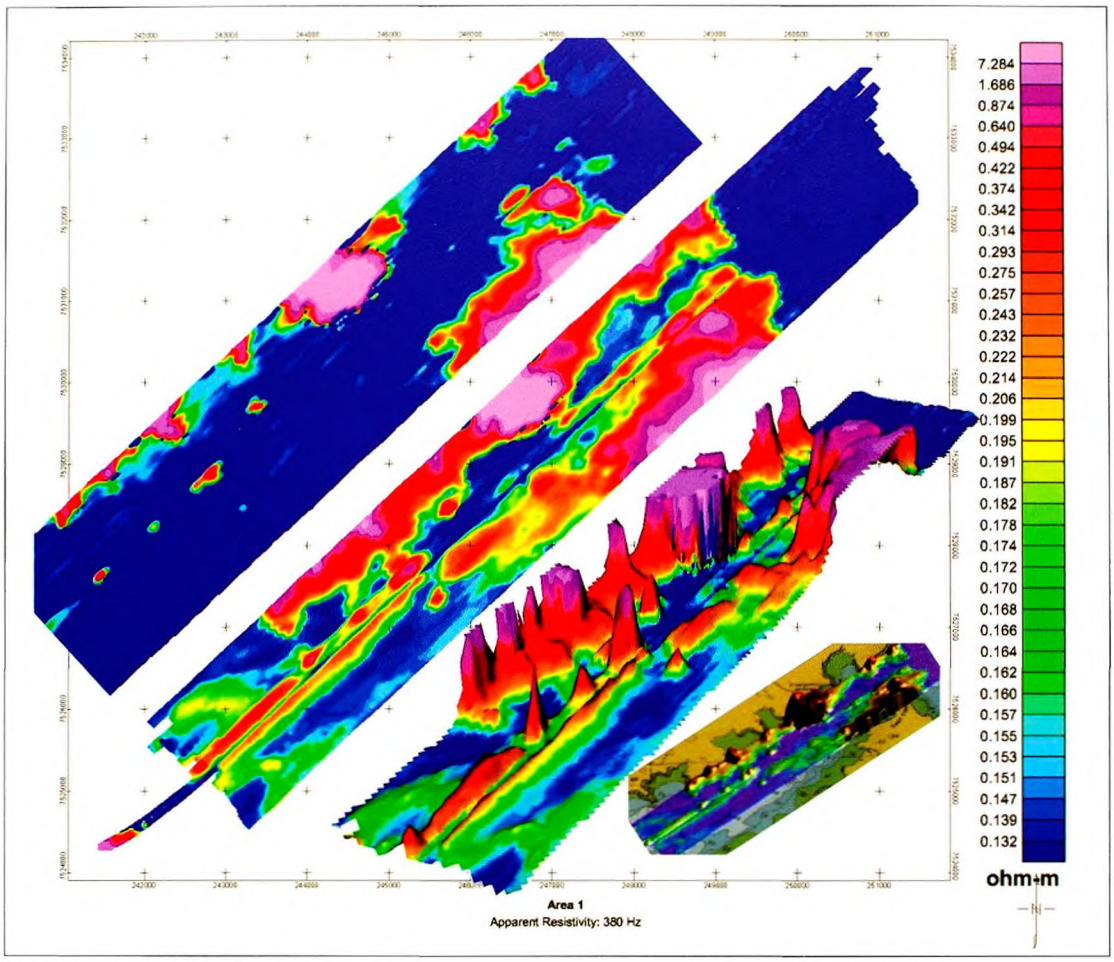

Figure 16: Apparent resistivity map, Area 1. Upper left inset: apparent resistivity at 1,537Hz; gridded map (centre): apparent resistivity at 387Hz, grid spacing 1,000m, both resistivity maps (1,537 and 387Hz) at same scale; lower right inset: 3D image of apparent resistivity (387Hz) where height is determined by the resistivity, note the 'drop' in resistivity in the NE corner where STP opens into the deeper sea. All three images use the same colour scale bar shown on right. Bottom right inset: semi-transparent apparent resistivity at 387Hz draped over AUS 260 showing correlation of regions of higher resistivity with shallow areas and submerged rocks. Unlike Figure 15, the survey area includes sections flown over land.

ly trace the variation in sea depth in waters surrounding Cape Naturaliste, and they also detect the deeper waters offshore from Cape Naturaliste. In this region of deeper seawater, the CDI section grossly underestimates the conductivity of the upper seawater layer. However, the boundary between layers having conductivity in the range 0.1 to 0.01 S/m and the more resistive basement, approximately tracks the known sea depth down to about 70m. The percent error of the estimated sea depths was found to be 6% using layered-earth inversion of inline component data in the depth range of 25 to 94m offshore Cape Naturaliste. A thorough discussion of root-mean square residual errors in different depth intervals and a comparison of inline and vertical component responses is given by Vrbancich et al. (2004b).

The CDI based on inline component data (dBx/dt) at 25Hz and 12.5Hz GEOTEM is presented in Figure 20 and shows that at 25Hz (Figure 20a) the sea depth is accurately determined down to 60m, whereas at 12.5Hz (Figure 20b), airborne EM is unsuitable for bathymetric mapping unless late-time system noise can be reduced. The GEOTEM system has a larger transmitter dipole moment, lower receiver noise and a

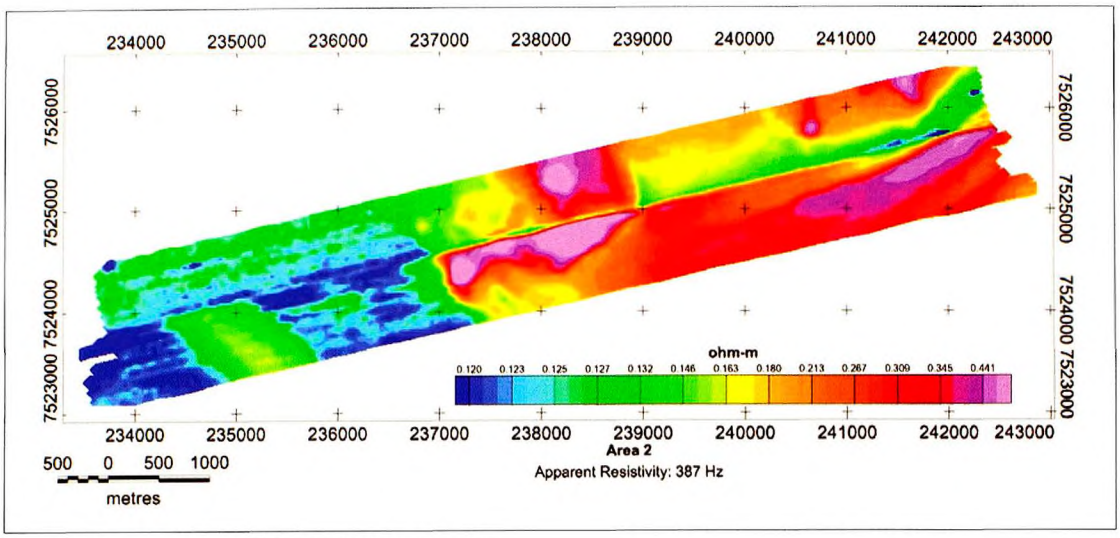

Figure 17: Apparent resistivity at 387Hz for Area 2.

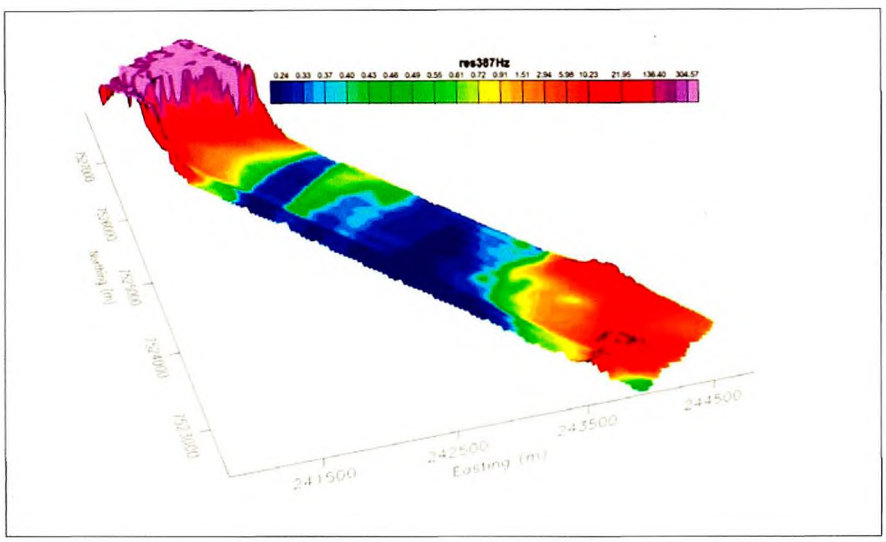

Figure 18: 3D representation of apparent resistivity at 387Hz for Area 3. Height is determined by resistivity value. The northern section (upper left) is the beach area on the Townshend Island shoreline, the southern area covers the beach approaches to Triangular Islands.

larger transmitter-receiver separation, compared to the QUESTEM system. These factors would restrict the QUESTEM system to shallower investigation depths compared to those obtained from the GEOTEM system. Layered-earth inversion studies for these GEOTEM surveys have not yet been completed. Vrbancich et al. (2004c) discuss inline and vertical component B-field and dB/dt component EM responses at 12.5 and 25Hz and the effects of transmitter-receiver geometry on error minimisation criteria used in the CDI processing program EMFlow.

Conclusions and Future Work

AEMB studies have relied on instrumentation developed for surveying over land. The AEMB surveys have all shown that it is possible to obtain seawater depths from the EM response measured over shallow water. Several examples taken from fixed-wing and helicopter surveys have been presented in this paper. However the AEM systems have not yet been optimised for marine surveying. This is a signifi-

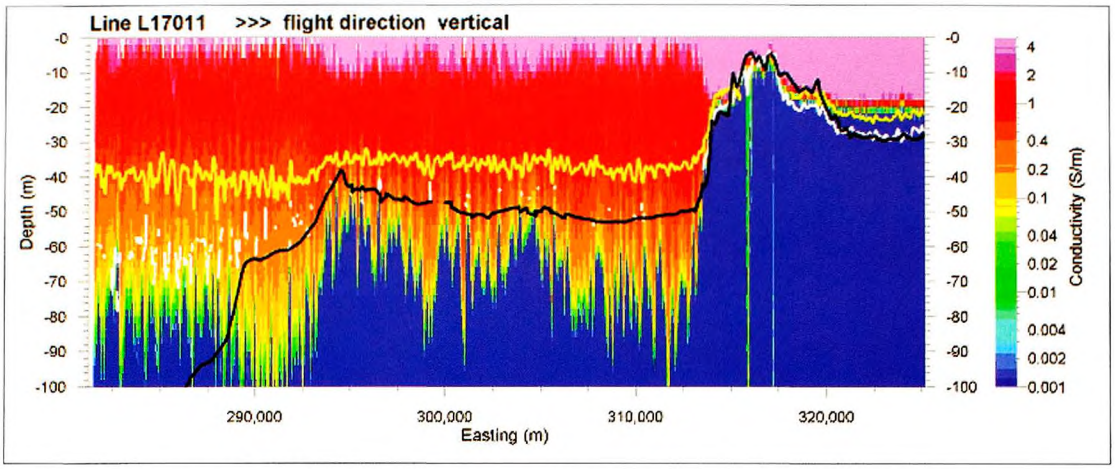

Figure 19: Conductivity-depth section (EMFlow) from vertical component data and layered-earth inversion depths (inline component: white, yellow; vertical component: cyan and grey profiles) for QUESTEM survey of Geograhe Bay and Cape Naturaliste. Cape Naturaliste is located west of Geographe Bay at about 315000 mE. Ground truth bathymetry profile (black) from gridded fairsheet data. Colour bar shows conductivity levels (S/m).

cant setback that means that the full potential of AEMB is not being realised. The following areas would be expected to lead to significant improvements in investigation depths, depth accuracy and the ability to discriminate between various sea bottom types based on interpreted resistivity: (i) lower FEM operating frequencies (or longer TEM delay times), (ii) lower survey altitudes, (iii) accurate measurements of the transmitter-receiver geometry, and (iv) improved inversion techniques.

Lower Survey Altitude

AEM is an active technique and the closer the transmitter and receiver is to the target, the greater the signal to noise ratio. The seawater surface is relatively flat, whereas terrestrial AEM survey regions are often rugged. Typical helicopter bird heights of 30 to 40m and fixed-wing bird heights of about 60 to 80m provide a safety margin for operators flying over land. Flying closer to the sea surface, either by flying the aircraft lower, or by increasing the vertical displacement between the bird and the aircraft, or both, is feasible from a safety viewpoint.

The magnitude of the primary magnetic field below the transmitter falls off as the cube of the distance (r) from the transmitter (Equations 1, 2), assuming a point dipole source (i.e., $1/r^3$). Furthermore, the secondary field also falls off approximately as the cube of the distance[4] between the induced currents in the ground and the receiver coil. Overall, there is a $\approx 1/r^6$ dependency for the secondary field detected at the receiver coil arising from the primary transmitted field. This field fall-off dependency is very approximate and assumes a uniform whole-space containing source and target and neglects the response of a layered half-space with conductive layers over a resistive basement. Nevertheless, small reductions in flight height would be expected to lead to significant increases in EM signal amplitude. Assume a standard bird height of 30m above sea level and 60m above sea bottom. By flying 10 m and 5 m above sea level, the signal from the seafloor is increased approximately by a factor of $(60/40)^6$ and $(60/35)^6$ i.e., 11.4 and 25.4 respectively[5]. If the seawater in this example were now 10 m deep, these factors would increase to 64 and 360 for flight heights of 10m and 5m above sea level respectively. Flying closer to seawater would however require a modification to the recording instrumentation to avoid signal saturation and improved

[4] The fall-off is not strictly proportional to $1/r^3$ because the target is not a "point" source, but rather a distributed source determined by the footprint size of the AEM instrumentation

[5] Numerically modelling a HCP system at 400 Hz above a 30 m seawater layer (at 4 S/m) overlying a resistive basement (0.01 S/m) leads to an increase in the in-phase/quadrature response by factors of 6.8/14.6 and 13.9/39.9 when the altitude drops from 30 m to 10 m and 5 m above sea level respectively

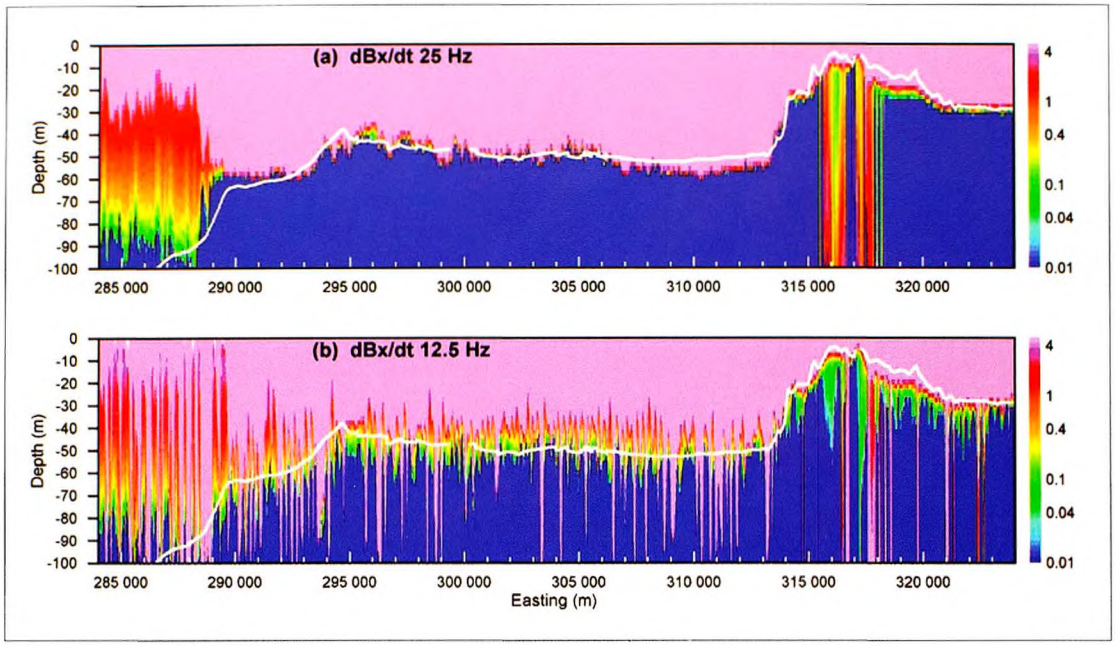

Figure 20: Conductivity-depth sections (EMFlow) for GEOTEM survey of Geograhe Bay and Cape Naturaliste. Cape Naturaliste is located west of Geographe Bay at about 315000 mE. Ground truth bathymetry profile (white), from gridded fairsheet data. (a): inline component at 25Hz, (b): inline component at 12.5Hz. Colour bar shows conductivity levels (S/m). Both lines cover the same flight path.

methods for accurately measuring the bird height above seawater. Lower survey altitudes may allow weaker transmitter moments to be used whilst maintaining current instrumentation sensitivities. This procedure raises the possibility of using unmanned aerial vehicles for AEMB.

Lower Operating Frequency

The lowest frequency is nominally about 400 Hz in helicopter FEM systems (Table 1). The skin depth (plane wave attenuation factor of *1/e*= 37%) in a conductor gives a reasonable "rule of thumb" estimate of the depth of penetration of AEM systems, which is about 2 skin depths. In seawater, the skin depth δ(m) at low frequencies (Equation 5) is given by $\delta \approx 500/\sqrt{\sigma f}$ where σ is the conductivity (S/m) and f is frequency (Hz). For seawater ($\sigma \approx$ 4 S/m), $\delta \approx 250/\sqrt{f}$. (The diffusion depth, $\delta_{TD} = \sqrt{(2t/\sigma\mu_0)}$, is a time domain equivalent of the skin depth, where t is the delay time and μ_0 is the magnetic permeability of free space.) Table 1 gives the skin depths for the DIGHEM^V Resistivity and DIGHEMV birds used to survey Sydney Harbour and Shoalwater Bay, together with two lower frequencies for comparison. Designing the AEM system to operate at lower frequencies (or longer delay times) is difficult because the introduction of low frequency noise may offset any gains to be made by increasing the skin depth or diffusion depth, for example, as shown by the 12.5Hz GEOTEM system for bathymetric mapping (Figure 20 and Vrbancich et al., 2004c). On the other hand, the increased investigation depths obtained by operating the lowest system frequency below 100Hz would be very beneficial for AEMB surveys. Such a system became operational in 1992 when the Through Ice Bathymetry System (TIBS) was developed under contract for the Canadian Hydrographic Service. TIBS was designed for marine use and could survey through seawater to depths of about 50 to 60m using frequencies ranging from 45 to 33000 Hz (Valleau and Holladay, 1987).

Dynamic Bird Offsets

To date, there appear to be few, if any, accurate positioning or ranging devices used in AEM to measure the transmitter-receiver geometry to sub-metre accuracy when surveying over seawater. In the case of fixed-wing TEM systems, the receiver located in the bird is towed behind the transmitter and swaying

motion leads to varying vertical, horizontal and transverse receiver offsets, as well as pitch, roll and yaw motions in both the receiver and transmitter. In the case of helicopter AEM systems, the transmitter and receiver are fixed within the same frame, however the combined system can still sway below the helicopter such that pitching and rolling motions may introduce errors in the assumed inline and vertical component EM responses. In addition to these unknowns, in both cases, the exact height of the bird above sea level is unknown as laser altimeters are not routinely used, or if they are, they are not reliable when flying over seawater. AEMB surveys assume a nominal fixed vertical and horizontal bird offset relative to the centre of the transmitter. The height of the bird above seawater at any given time is assumed to be the difference between the radar altimeter recording of the aircraft and the fixed vertical bird offset. Unknown variable transmitter-receiver geometry can significantly affect the accuracy of seawater depths obtained from AEM measurements. Vrbancich and Smith (2004d) studied the effect of seawater proximity on computed dynamic bird offsets obtained from corrected primary fields recorded at the receiver, for GEOTEM surveys in Geographe Bay. Vrbancich and Smith (2004d) found distinct differences between (i) the averaged dynamic bird offsets and the assumed nominal fixed bird offset, and (ii) averaged dynamic offsets obtained from survey data recorded over seawater and at high altitude. Introducing dynamic bird offsets in the inversion and CDI processing would be expected to improve the accuracy of AEMB mapping.

Joint Inversion of Multi-component Data

The limitations in determining bird position and altitude over seawater using the corrected primary field method may be overcome by performing joint inversion of the three recorded components (inline, vertical and transverse) of the EM response and the recorded pitch and roll angles of the transmitter loop. The joint inversion includes the receiver pitch and horizontal and vertical bird offsets as variable model parameters. This approach is being developed at Fugro Airborne Surveys, and is being tested with AEM survey data taken recently in Torres Strait (Figure 2) using the 25Hz GEOTEM system (Sattel et al., 2004). Within the surveyed area of Torres Strait, the sea depth profiles obtained from joint inversion of multi-component data are more accurate than the depth estimates obtained from CDI processing that assumes a nominal fixed bird offset.

Concluding Comments

The vertical and horizontal resolution is of fundamental importance for hydrographic surveying. The AEMB horizontal resolution is dependent on the electromagnetic footprint and whilst this has been estimated within certain approximations, it cannot necessarily be applied directly because (i) features at a smaller scale than the footprint can be detected if there is a resistivity contrast, and (ii) the footprint calculations assume a homogeneous ground. In reality, bathymetric mapping using AEM covers areas where there is layering and also where the seafloor is not flat. Advanced 2D/3D electromagnetic modelling could be used to study the effects of channels and ridges on the AEM response and these studies are in progress. Interpreting the AEM response from data recorded over areas where the seafloor topography is variable over short distances will provide an experimental measure of the horizontal resolution that can complement EM numerical modelling studies.

The vertical resolution can be estimated from the AEMB and ground-truth depth profiles shown in this report. The variable residual error is almost certainly caused by instrumentation errors and variable transmitter-receiver geometry that needs to be adequately accounted for when deriving depth estimates from the EM response. In shallow water between 25 to 35m depth, having a Root Mean Square (RMS) depth of 31.1m, the RMS error was found to be 0.9m and 1.3m respectively for inline and vertical component EM data respectively. The RMS error was computed from the residual difference between the accurate ground truth and estimated AEMB depth at each of the 5,800 samples taken from thirteen flight lines traversing Geographe Bay (Vrbancich et al., 2004b). In deeper water within the depth range of 25 to 92m (RMS depth of 54 m), the RMS error from 2,039 samples flown offshore from Cape Naturaliste was 4.7m, and 3.2m for 1865 samples on the return flight (Vrbancich et al., 2004b). Sub-metre water depth accuracies were achieved with DIGHEM surveys of Sydney Harbour, down to depths of about 20m although the residual error was not consistent at these depths (Vrbancich et al., 2000a). Valleau and Holladay (1987) showed that

'water depths and ice thickness can be determined to an accuracy of 10cm or better, and deeper water can be sounded at depths of up to 100 metres in typical seawater'. With improvements in instrumentation and especially with developments to account for variable transmitter-bird geometry effects, there is every expectation that substantial improvements in the vertical resolution can be achieved.

It is envisaged that the application of AEMB for hydrographic reconnaissance in open shallow coastal waters, particularly those affected by turbidity, could be carried out using a fixed-wing TEM system. Helicopter AEMB could also be used to support rapid environmental assessment of harbours, choke points and approaches to beaches where chart information is outdated or unreliable.

Acknowledgements

I gratefully acknowledge the contributions made by my coauthors in the development of AEMB for investigating Australian coastal waters. I also acknowledge the support and sponsorship of the Australian Hydrographic Service throughout these studies, and for permission to use a section of AUS260 in Figure 14. I thank Capt. Robert Ward (RAN) for helpful comments on this report. I thank Fugro Airborne Surveys for permission to use their photos of the GEOTEM and DIGHEM systems in Figures 4 and 5.

References

Anderson, W.L. (1979), Computer program – numerical integration of related Hankel transforms of orders 0 and 1 by adaptive digital filtering, *Geophysics*, 44, 1287-1305

Becker, A., Liu, G., and Morrison, H.F. (1987), Airborne electromagnetic sensing of sea ice thickness, *Univ. Calif., Berkeley, final contract report to USACRREL*

Becker, A., and Liu, G. (1988), Airborne electromagnetic sensing of sea ice thickness, *Univ. Calif., Berkeley, final contract report to NORDA*

Bennett, R.H., Lambert, D.N., Hulbert, M.H., Burns, J.T., Sawyer, W.B. and Freeland, G.L. (1983), Electrical resistivity/conductivity in seabed sediments, in Geyer, R.A., Ed., *CRC Handbook of Geophysical Exploration at Sea: CRC Press*

Bergeron, C.J., Ioup, J.W., and Michel, G.A. (1989), Interpretation of airborne electromagnetic data using the modified image method, *Geophysics*, 54, 1023-1030

Bryan, M.W., Holladay, K.W., Bergeron, C.J., J.W. Ioup, and G.E. Ioup (2003), MIM and non-linear least-squares inversions of AEM data in Barataria basin, Louisiana, *Geophysics*, 68, 1126-1131

Emerson, D.W., and Phipps, C.V.G. (1969), The delineation of the bedrock configuration of Port Jackson, New South Wales, with a boomer system, *Geophysical Prospecting, 17*, 219-230

Fountain, D. (1998), Airborne electromagnetic systems – 50 years of development, *Exploration Geophysics, 29,* 1-11

Frischknecht, F.C. (1967), Fields about an oscillating magnetic dipole over a two-layer earth, and application to ground and airborne electromagnetic surveys, *Quarterly of the Colorado School of Mines, 62*, 1-165

Fullagar, P.K., and Oldenburg, D.W. (1984), Inversion of horizontal loop electromagnetic frequency soundings, *Geophysics*, 49, 150-164

Fullagar, P.K., and Reid, J.E. (1992), Conductivity-depth transformation of fixed-loop TEM data, *Exploration Geophysics*, 23, 515-520

Harris, G.A., Vrbancich, J., Keene, J., and Lean, J. (2001), Interpretation of bedrock topography within the Port Jackson (Sydney Harbour) region using marine seismic reflection, *Extended Abstracts, ASEG 15th Geophys. Conf.*, Brisbane, Aug. 2001

Jackson, P.D., Taylor Smith, D. and Stanford, P.N. (1978), Resistivity-porosity-particle shape relationships for marine sands: *Geophysics, 43*, 1250-1268

Johansen, H.K., and Sorensen, K. (1979), Fast Hankel transforms, *Geophysical Prospecting, 27*, 876-901

Kovacs, A., and Holladay, J.S. (1990), Sea-ice thickness measurement using a small airborne electromagnetic sounding system, *Geophysics, 55*, 1327-1337

Kovacs, A., Holladay, J.S., and Bergeron, C.J. (1995), The footprint/altitude ratio for helicopter electromagnetic sounding of sea-ice thickness: comparison of theoretical and field estimates, *Geophysics, 60*, 374-380

Lane, R., Plunkett, C., Price, A., Green, A., and Hu, Y. (1998), Streamed data – a source of insight and improvement for time domain airborne EM, *Exploration Geophysics, 29*, 16-23

Lane, R., Green, A., Golding, C., Owers, M., Pik, P., Plunkett, C., Sattel, D., and Thorn, B. (2000), An example of 3D conductivity mapping using the TEMPEST airborne electromagnetic system, *Exploration Geophysics, 31*, 162-172

Liu, G., and Becker, A. (1990), Two-dimensional mapping of sea ice keels with airborne electromagnetics, *Geophysics, 55*, 239-248

Macnae,J., and Lamontagne, Y. (1987), Imaging quasi-layered conductive structures by simple processing of transient electromagnetic data, *Geophysics, 52*, 545-554

Macnae, J., Smith, R., Polzer, B.D., Lamontagne, Y., and Klinkert, P.S. (1991), Conductivity-depth imaging of airborne electromagnetic step-response data, *Geophysics, 56*, 102-114

Macnae. J., Robb, T., and Vrbancich, J. (2004), Rapid estimation of seawater depth from airborne electromagnetics, *submitted for publication in Exploration Geophysics*

Morrison, H.F., and Becker, A. (1982), Analysis of airborne electromagnetic systems for mapping depth of seawater, *Final report, ONR contract no. N00014-82-M-0073*

Raiche, A., Sugeng, F., and Xiong, Z. (1996), Modelling complex structures using thin sheet approximation, *Conference Volume for the 13th Workshop on Electromagnetic Induction in the Earth*, Onuma, Japan, 107-108

Raiche, A. (1999), A flow through Hankel transform technique for rapid accurate Green's function computation, *Radio Science, 34*, 549-555

Reid, J.E., and Vrbancich, J. (2004), A comparison of the inductive-limit footprints of airborne electromagnetic configurations, *Geophysics, 69*,1229-1239

Sattel, D., Lane, R., Pears, G., and Vrbancich, J. (2004), Novel ways to process and model GEOTEM data, *Extended Abstracts, ASEG 17th Geophys. Conf.*, Sydney, Aug. 2004

Smith, R.S., and Annan, A.P. (1997), Advances in airborne time-domain EM technology: in Gubbins, A.G., Ed., *Proceedings of Exploration 97: Fourth Decennial International Conference on Mineral Exploration*, 497-504

Valleau, N.C., and Holladay, J.S. (1987), Airborne electromagmetics for through ice bathymetry, *Canadian Hydrographic Conference*, Burlington, Ontario, Feb., 17-19

Vrbancich, J., Hallett, M., and Hodges, G. (2000a), Airborne electromagnetic bathymetry of Sydney Harbour, *Exploration Geophysics, 31*, 179-186

Vrbancich, J., Fullagar, P.K., and Macnae, J. (2000b), Bathymetry and seafloor mapping via one dimensional inversion and conductivity depth imaging of AEM, *Exploration Geophysics, 31*, 603-610

Vrbancich, J., Reid, J., Annetts, D., Pfaffling, A., and Worby, A. (2004a), 3D EM modelling of Antarctic sea ice pressure ridges, *Extended Abstracts, ASEG 17th Geophys. Conf.*, Sydney, Aug. 2004

Vrbancich, J., Sattel, D., Annetts, D., Macnae, J., and Lane, R. (2004b), A case study of AEM bathymetry in Geographe Bay and over Cape Naturaliste, Western Australia: Part 1 - 25 Hz QUESTEM, *submitted for publication in Exploration Geophysics*

Vrbancich, J., Macnae, J., Sattel, D., and Wolfgram, P. (2004c), A case study of AEM bathymetry in Geographe Bay and over Cape Naturaliste, Western Australia: Part 2 - 25 Hz GEOTEM, *submitted for publication in Exploration Geophysics*

Vrbancich, J., and Smith, R. (2004), Dynamic bird offsets from 25 and 12.5 Hz GEOTEM surveys over seawater, *submitted for publication in Exploration Geophysics*

Vrbancich, J., and Fullagar,P.K. (2004), Seawater depth determination using the helicopter HoisTEM system, *submitted for publication in Exploration Geophysics*

Wait, J.R.(1982), Geo-Electromagnetism, Academic Press

Wolfgram, P., and Karlik, G. (1995), Conductivity-depth transform of GEOTEM data, *Exploration Geophysics, 26*, 179-185

Won, I.J., and Smits. K.(1986), Characterisation of shallow ocean sediments using the airborne electromagnetic method: *IEEE J. Oceanic Eng., OE-11*, 113-122

Zollinger, R., Morrison, H.F., Lazenby, P.G., and Becker, A. (1987), Airborne electromagnetic bathymetry, Geophysics, 52, 1127-1137

Biography

Julian Vrbancich joined the Defence Science and Technology Organisation (DSTO) at Pyrmont (Sydney) in late 1984 and investigated ElectroMagnetic (EM) emissions and static electric fields arising from corrosion currents in ships. Since about 1997, Julian began investigating the use of Airborne EM (AEM) methods to explore shallow water marine environments to measure sea depth and map seafloor resistivity. This work has also extended to include the use of AEM for sea ice thickness measurements in Antarctica.

E-mail: julian.vrbancich@dsto.defence.gov.au